Influence of soil parameter spatial variability on railway loess-filled embankment settlement

Yanjie Zhang[1]; Yuanyuan Zhang[2]; Xu Wang [3]; Hanxing Zhu[4]; Chunxiang Guo [5]

[1]Associate professor, School of Civil Engineering, Lanzhou Jiaotong University, Lanzhou 730070, China. Email: zhangyanjie@lzjtu.edu.cn (corresponding author)

[2]M.D. Student, School of Civil Engineering, Lanzhou Jiaotong University, Lanzhou 730070, China. Email: zyy060619@163.com

[3]Professor, National and Provincial Joint Engineering Laboratory of Road &Bridge Disaster Prevention and Control, Lanzhou Jiaotong University, Lanzhou, 730070, China. Email: publicwang@163.com

[4]Reader, School of Engineering, Cardiff University, Cardiff CF24 3AA, UK. Email: ZhuH3@cardiff.ac.uk

[5]Associate professor, School of Civil Engineering, Lanzhou Jiaotong University, Lanzhou 730070, China. Email: guocx@mail.lzjtu.cn

Keywords: Railway embankment; Spatial variability; Random field; Monte Carlo simulation; Settlement

Abstract: This study involved an embankment settlement analysis of a case study of the railway loess-filled embankment section of the Baozhong railway in Guyuan, China. The two-dimensional spatial variability of the soil parameters in the embankment fill layer was simulated using random field theory and the finite difference method. The covariance matrix decomposition method was used to discretize the soil parameters within different geological cells. Settlement predictions were evaluated through Monte Carlo simulations with varying

horizontal scale of fluctuations (SOFs), and the embankment surface settlement values at the centerline were compared to the deterministic calculation model (DCM), random variable model (RVM), and random field model (RFM). The results indicated that the horizontal SOFs ranging from 40–60 m in the loess-filled embankment can effectively capture the spatial distribution pattern of the soil parameters. Spatial variability exerts a substantial influence on embankment settlements. Neglecting the spatial variability of soil properties underestimates the risk of surface settlement in embankments compared to the DCM. Therefore, RFM analysis that considers the spatial variability of soil parameters must be incorporated to ensure safe operation and design in subgrade engineering.

Introduction

Due to long-term geological and climatic changes, the Loess Plateau in western China has formed numerous loess gullies and mountain valleys. Given the significant variation in terrain elevation, construction projects for railways and highways require a large number of embankments to meet linear requirements (Liang et al. 2022; Zhu and Li. 2020). The settlement of a subgrade during its service life must remain within design limits to ensure adequate serviceability and safety. In railway subgrade engineering, excessive differential settlement can lead to an undesirable increase in the dynamic forces on the tracks, resulting in a suboptimal performance of the slabs and ballast (Charoenwong et al. 2022; Zhai 2007; Zhou et al. 2020). In highway subgrade engineering, excessive settlement can lead to pavement cracking or displacement, compromising vehicle comfort and safety (Chai and Miura 2002; Lu et al. 2020). Consequently, efficient analysis and calculation of settlement in filled embankments has become a pivotal research topic in subgrade construction. The settlement of subgrade is primarily attributed to the compression of materials utilized for embankment filling, which depends on their compressibility characteristics. Consequently, differential settlements arise due to disparities in compressibility.

Numerous studies have investigated subgrade settlement performance using numerical analysis (Tian et al. 2023; Zhuang and Wang 2016), analytical methods (Chen et al. 2016; Feng and Lei 2022), model experiments (Bian et al. 2021; Chen et al. 2014), and case studies (Peduto et al. 2017; Xiao et al. 2023). These studies have partially addressed the deformation and settlement response of subgrades by considering various factors, such as foundation types, foundation reinforcement methods, soil properties, soil-filled height, groundwater levels, and traffic loading. Engineers directly assess differences in settlement by considering the design embankment geometry and composition (Foye and Soong 2010). However, comprehensive evaluation of subgrade settlement variations is limited due to the high costs associated with sampling and testing. Consequently, conventional state-of-the-art methodologies for mathematically modeling settlement treat the subgrade materials as homogeneous, despite the inherent heterogeneity of soil in reality (Phoon and Kulhawy 1999; Wang et al. 2018; Zhang et al. 2021b). The spatial variability of soil properties leads to strain localization along neighboring weak zones, resulting in unpredictable differential settlement when assuming soil homogeneity. (Li et al. 2016; Pan et al. 2021; Sun et al. 2022). During subgrade filling, the geological and historical information of the original soil is lost, and its natural structure is destroyed. Additionally, the complex material composition and various filling methods result in embankments with intricate engineering geology and hydrogeological characteristics (Zhang et al. 2021a; Yao et al.2021), as well as significant spatial variability and uneven distribution

(Elkateb et al. 2003; Juang et al. 2019; Phoon and Ching 2015).

In geotechnical engineering, the modeling of soil property spatial variability has predominantly relied on random field theory. Vanmarcke (1977) was the first to discuss the impact of soil spatial variability on geotechnical systems using the random field method. Subsequently, extensive attention has focused on various aspects of geotechnical engineering through random field analyses, including slope stability (Cho 2007; Deng et al. 2022; Kalantari et al. 2023; Kim and Sitar 2013; Nguyen et al. 2019), foundation capacity and settlement (Fenton and Griffiths 2003; Li et al. 2016; Simões et al. 2020), and tunnel deformation performance (Huang et al. 2015; Zhang et al. 2021b; Zhang et al. 2024). Several studies have been conducted on the impact of spatial variability on subgrade engineering (Luo and Bathurst 2018b; Sun et al. 2022; Vaillancourt et al. 2015). For example, Vaillancourt et al. (2015) demonstrated through finite difference modeling that the significant variability in subgrade soil affects the long-wavelength pseudo-profile of roads at the completion stage. Luo and Bathurst (2018b) used random finite element modeling to consider the spatial variability of soil parameters and presented the load-settlement characteristics of a geogrid-reinforced large embankment. Sun et al. (2022) investigated the effects of the spatial variability in cement-treated soil on airport pavement roughness, finding that random spatial variability increased settlement, which further increased with a higher coefficient of variation.

In summary, previous research has suggested that settlements are significantly influenced by the spatial variability of soil parameters. However, a comprehensive literature review revealed that no studies have analyzed railway loess-filled embankments while considering the spatial variability of soil parameters. To investigate the spatial variability of subgrade soil parameters on the settlement deformation of railway loess-filled embankments, this study combined a finite difference element (FDE) method with a random field model (RFM), utilizing cone penetration test (CPT) data and geotechnical test parameters from the K329–K331 section of the Baozhong railway subgrade. RFM discretization of the soil parameters within different geological cells was achieved using covariance matrix decomposition (CMD). Consequently, a two-dimensional embankment model was established in which the FDE was aligned with random cells to consider the random field. The influence of the spatial variability on settlement was studied by comparing the embankment surface settlement values at the centerline under three models: deterministic calculation model (DCM), random variable model (RVM), and RFM. These findings provide valuable insights for ensuring safe operation and design in subgrade engineering.

Computational Framework

Spatial variability of soil properties

In geotechnical engineering, it is not feasible to acquire the soil parameters directly at each point in the soil profile for a specified geological cell (or soil layer). Random field theory effectively characterizes the inherent variability of soil parameters using a correlation coefficient between any two discrete points. Various methods exist for generating realizations of random fields, including the local average subdivision (Alamanis and Dakoulas 2021; Fenton and Griffiths 2007), fast Fourier transformation (Li et al. 2021; Zhu et al. 2013), CMD (Gong et al. 2020; Yang et al. 2021), turning-band method (Mantoglou and Wilson 1982; Pardo-Igúzquiza and Chica-Olmo 1993), K-L expansion (Huang et al. 2001; Wang et al. 2018), and sequential Gaussian simulation (Pebesma 2004; Wang et al 2021). CMD involves constructing a covariance matrix for a random field and subsequently performing Cholesky decomposition to obtain the upper and lower triangular matrices. This approach is simple to implement and accommodates random fields with irregular geometries without additional computational effort. Additionally, it requires only one matrix decomposition for Monte Carlo simulations (MCS), as generating each additional realization requires only backward substitution (Fenton 1999; Jiang ang Huang 2016; Nguyen et al 2021). Therefore, CMD was preferred in this study. CMD uses an autocorrelation function (ACF) to quantify the correlation coefficient between two points located at any distance within each soil layer. Various types of theoretical ACFs, such as the single exponential, squared exponential, cosine exponential, binary noise, and second-order Markov, are commonly employed to describe the spatial autocorrelation of soil parameters (Phoon et al. 2003; Kim and Sitar 2013). The single exponential function has been extensively utilized to study the impact of spatial variability in soil parameters due to its simplicity and ease of establishment in random fields (Cami et al. 2020; Li et al. 2016; Zhang et al. 2022). In this study, a single exponential ACF was used to model the spatial variability of the soil parameters. The ACF can be expressed by Eq. (1)

$$\rho(\tau_x, \tau_z) = \exp\left[-2\left(\frac{\tau_x}{\delta_h} + \frac{\tau_z}{\delta_v}\right)\right] \tag{1}$$

where ρ (τ_x, τ_z) is the correlation coefficient between two arbitrary points in a soil layer; τ_x and τ_z are the horizontal and vertical distances between two points in space, respectively; and δ_h and δ_v are the horizontal and vertical scale of fluctuation (SOF) of soil parameters, respectively.

The correlation function value between any two arbitrary points can be derived using the SOF as described in Eq. (1). The CMD method requires defining a discrete set of n points at which the random field can be sampled. Subsequently, a covariance matrix, $\boldsymbol{C}_{n\times n}$, quantifying the correlation between all of the sampling points, is constructed. This matrix is a positive definite symmetric matrix (Yang et al., 2022). The Cholesky decomposition (Press et al. 2007) is expressed as:

$$\boldsymbol{C}_{n\times n} = \boldsymbol{MU} = \boldsymbol{MM}^{\mathrm{T}} \tag{2}$$

$\boldsymbol{M}$ is the lower triangular matrix, while $\boldsymbol{U}$ is the upper triangular matrix, $\boldsymbol{U}=\boldsymbol{M}^{\mathrm{T}}$.

An autocorrelated standard normal random field $\boldsymbol{Q}$ is obtained by

$$\boldsymbol{Q} = \boldsymbol{MY} \tag{3}$$

where the vector $\boldsymbol{Y}$ consists of a sequence of independent standard normal random variables. The lognormal distribution can effectively capture the random distribution without generating negative values for soil parameters (Huang et al. 2015; Phoon and Ching 2015). The lognormal distributed random field $\boldsymbol{F}$ can be generated by

$$\boldsymbol{F} = \exp\left(\mu_{\ln i}\boldsymbol{I} + \sigma_{\ln i}\boldsymbol{Q}\right) \tag{4}$$

where $\boldsymbol{I}$ represents an n-dimensional column vector in which all elements are unity, $\mu_{\ln i}$ and $\sigma_{\ln i}$ are the mean and standard deviation of normal random field ln($\boldsymbol{F}$), respectively.

$$\mu_{\ln i} = \ln \mu_i - \sigma_{\ln i}^2 / 2 \tag{5}$$

$$\sigma_{\ln i} = \sqrt{\ln\left[1 + \left(\sigma_i / \mu_i\right)^2\right]} \tag{6}$$

Vertical scale of fluctuation (δ_v)

In random field theory, the statistical characterization of the spatial variability of a parameter includes its mean, variance (standard deviation), and SOF (Vanmarcke 1977). The SOF plays a crucial role in capturing the inherent spatial variability within random fields (Huang et al. 2015; Zhang et al. 2022). This study adopted the semivariogram function because it can yield accurate results with fewer samples and less stringent constraints on sampling intervals (Phoon and Ching 2015). Denoting the sample size of the soil parameters as m, the specific steps for calculating the fluctuation range using the semivariogram method are outlined below:

(1) The semivariogram value $\gamma^*(h)$ was calculated by applying formula (7) with a given lag distance $h = j\Delta z,\ j = (0, 1, \cdots, m-1)$.

$$\gamma^*(h) = \gamma^*(j\Delta z) = \frac{1}{2(m-j)} \sum_{i=1}^{m-j} \left[X(z_{i+j}) - X(z_i) \right]^2 \tag{7}$$

Where $X(z_i)$ and $X(z_{i+j})$ are the observed values of X at z_i and z_{i+j}, and $(m$-$j)$ is the number of pairs of data points separated by the lag h, or the number of paired comparisons (Kerry and Oliver 2011).

(2) Plot the $\gamma^*(h)$~h correspondence diagram. A typical theoretical spherical semivariogram is presented in Fig. 1. The experimental semivariogram is characterized by three parameters (Clark 1979; Onyejekwe et al. 2016): nugget effect (D_0), sill ($D + D_0$), and range of influence (a). Spherical, exponential, and Gaussian theoretical semivariogram models were used for curve fitting.

(3) The vertical SOF (δ_v) was evaluated by a fitting a best-fit continuous theoretical semivariogram model obtained in step (2). The relationship between range of influence (a) and SOF for some models are presented Table 1. By selecting the function model with the largest coefficient R^2, the fluctuation range of the soil parameters and shear wave velocity in various boreholes were determined.

Project overview

The Bao Zhong railway, which connects Baoji in Shaanxi to Zhongwei in Ningxia, was completed and officially operated in July 1996. The study area is situated in the Malian town of Guyuan City (Fig. 2) within Ningxia Province along the K329–K331 section of the Baozhong railway. Guyuan City lies on the northwestern periphery of the Chinese Loess Plateau and experiences a semi-arid and semi-humid continental climate, with precipitation mainly occurring in the summer. Approximately 70% of the annual rainfall is concentrated between June and September. Due to water scarcity, large-scale farmland irrigation is required every spring and autumn for agricultural crops, leading to a rise in groundwater levels. Consequently, an increase in the prevalence of loess disease has been observed along railway lines (Fig. 3). Based on the corresponding data, since 2003, extensive flood irrigation of farmland has induced the settlement and gradual elevation of railway subgrades. After years of subsidence, uneven settlement occurred within the railway subgrade, leading to track irregularities (Fig. 3c and d) accompanied by many cracks on both sides of the roadbed (Fig. 3a and b). The longest crack extends to approximately 600 m. Therefore, urgent action is needed to address the settlement issue of the Baozhong railway subgrade loess (Zhao et al. 2020).

Geological engineering conditions

The embankment primarily comprises loess mixed with fill, exhibiting significant variability due to long-term irrigation, rainfall infiltration, vehicle load, dry-wet cycles, freeze-thaw cycles, and other factors. The ground soil beneath the embankment can be divided into two distinct layers: the upper layer includes a cohesive soil deposited in modern lake facies, whereas the lower layer is composed of gravel silty clay deposited in river facies. The specific lithological characteristics of each stratum are as follows:

(1) Silty clay

The silty clay was yellowish-brown and hard plastic with no clear bedding characteristics. It has high dry strength and medium toughness without any rocking reaction. The soil contained F_e, M_n, and small amounts of oxides. The thickness of the soil layer ranges from 3.9 – 8.4 m.

(2) Silt

The silt layer exhibits purple-red or light-yellow color and ranges from plastic to hard plastic in consistency. It has a low strength but medium toughness without any shaking reactions. The section appears smooth and contains F_e, M_n, and small amounts of oxides. When twisted by hand, the sand could be felt strongly within the silt layer, which had a thickness of 2.7 – 5.8 m. The physical and mechanical indices of each soil layer are listed in Table 2.

Embankment fill test

CPT and borehole tests were conducted along the shoulders of K330 + 000, K330 + 100, K330 + 150, K330 + 200, and other mileages. The test points were positioned at the top of the subgrade, as shown in Fig. 4. The physical and mechanical parameters of the embankment fill layer at K330 + 000 are presented in Table 3.

Vertical scale of fluctuation (δ_v) Analysis

To satisfy the requirements of a stationary random field, detrending was employed on the borehole data to obtain the fluctuation component, and the vertical SOFs were calculated using the semivariogram method. The vertical SOFs were determined based on both penetration resistance of CPT and borehole test data, with sampling intervals of 0.1 and 0.5 m, respectively. Table 4 lists vertical SOFs.

The negligible differences in the fluctuation ranges of various physical and mechanical parameters within the same borehole are illustrated in Fig. 5, indicating the inherent stability of soil attributes in a given area. The calculated fluctuation ranges for physical and mechanical parameters were 0.87, 0.84, 0.92, and 0.74 m with an average value of 0.84 m. In contrast, the fluctuation ranges derived from CPT data were slightly lower at 0.78, 0.74, 0.84, and 0.68 m with an average value of 0.76 m. This discrepancy arises because the sampling interval for geotechnical test parameters was 0.5 m, whereas the sampling interval for CPT was 0.1 m. The size of the sampling interval significantly affects the calculation results of the fluctuation range. (Lloret-Cabot et al. 2014; Sasanian et al. 2019). Moreover, there was a disparity in the sample sizes between the CPT and geotechnical test parameters, which also influenced the computation of the fluctuation range (Dasaka and Zhang 2012).

The vertical SOFs of physical and mechanical parameters in the calculated semivariograms indicate varying degrees of spatial dependence. In geotechnical engineering, the spatial average of a soil property over a specific domain is often more relevant and serves as a design parameter (Zhao et al. 2013). To compare dispersion among different soil properties conveniently and appropriately, it is advantageous to express variance without units. The coefficient of variation (COV) provides a useful and meaningful index for comparing variability among different properties (Wilding and Drees 1983).

The COV for a point (COV_p) is calculated by normalizing the standard deviation of the point with respect to its mean value (COV_p = point standard deviation / point mean). The spatial average COV (COV_a) is defined as follows (Zhao et al. 2013):

$$COV_a = \Gamma(L) COV_p \tag{8}$$

where $\Gamma^2(L)$ is a variance reduction function, L is the averaging length.

The approximate variance reduction function has been proposed for practical application (Vanmarcke 1983):

$$\Gamma^2(L) = \delta_v / L \tag{9}$$

The COV for physical and mechanical parameters is presented in Table 5. In the field of geotechnical engineering, it is widely acknowledged (Harr 1987; Gomes and Garcia 2002) that the variability of a property can be classified based on the magnitude of COV, which may be categorized as low (< 10%), medium (10 – 20%), high (20 – 30%), or very high (> 30%). Accordingly, the theoretical COV_a for physical parameters such as natural density, water content, and void ratio range from 4.2 – 4.8%, 1.4 – 1.7%, and 3.7 – 4.1%, respectively, indicating low variability in these properties. Based on the COV_p values, it can be observed that water content and void ratio exhibit medium variability, while natural density demonstrates significantly less variability compared to other physical properties. The natural density of soil is highly influenced by the specific gravities of soil minerals, which typically vary within a narrow range. The COV_a values for mechanical parameters, including cohesion, friction angle, and compression modulus, demonstrate variations ranging from 20.4 – 21.7%, 10.2 – 11.6%, and 5.3 – 6.0% respectively. The cohesion displays a high degree of variability while the compression modulus exhibits low variability. In case of embankment fill materials, the mean friction angle usually ranges between 20° and 40° with an associated COV_a varying from 5 – 15%. Considering potential measurement errors caused by variations in water content and dry density among soil specimens (Singh and Lee 1970), both cohesion and friction angle display very high levels of variability according to their respective COV_p values. Phoon and Kulhawy (1999) reported a range of 20 – 80% for clay, while the COV for mechanical parameters exhibits comparable magnitudes.

The COV_p indicate a wide range of variability, spanning from low to very high, while the COV_a denotes variability in soil parameters that can range from low to high. Increasing the sample size used for averaging the property will result in a reduction of the COV_a for the average soil property (Zhang et al. 2008; Zhao et al. 2013). Determining COV_p and COV_a values for typical loess fill properties can assist engineers in comprehending the inherent soil variability when estimating common design characteristics of embankments.

Horizontal SOF (δ_h) analysis

The horizontal SOF (δ_h) is impossible to calculate directly owing to the lack of sample data in the horizontal direction. In general, δ_h is greater than δ_v (Phoon and Kulhawy 1999). The ratio of the two ($N=\delta_h / \delta_v$) is a key parameter with significant influence. The range for δ_v in CPT results is relatively narrow, ranging from 0.06 – 2.6 m. However, the range for δ_h is fairly broad, ranging from 0.14 – 80 m (Phoon and Kulhawy 1999; Onyejekwe et al. 2016). Considered N values of 10, 30, 50, 70, and 100. Subsequently, the impact of varying N values on the settlement calculation was investigated.

Implementation procedure

RFM is commonly integrated with MCS and applied in engineering applications. MCS has been extensively utilized to analyze slope stability and foundation settlement in geotechnical engineering. This method is suitable for simulating independent and correlated geotechnical engineering parameters (Peng et al. 2017; Pan et al. 2021; Nguyen et al. 2021; Zhang et al. 2024). The simulation steps for the embankment settlement analysis were predicted as follows:

(1) The parameters of the random field, including bulk modulus (K), shear modulus (G),

cohesion, friction angle, and natural density were generated using CMD.

(2) A numerical model was established using the FISH programming language embedded in FLAC3D. Subsequently, the parameters in the RFM were individually mapped to a finite difference cell, and ultimately, the embankment settlement was calculated as a single result from a random simulation.

(3) These steps were repeated multiple times to obtain settlement data, considering the spatial variability of the soil parameters. The distribution pattern of these data was tested and compared with the deterministic analysis and calculation results that consider the vertical variability of the soil parameters.

Numerical model

The K330 + 000 section of the Baozhong Railway was used to establish the numerical model. Considering the symmetrical nature of the embankment, only half of it was modeled and analyzed using the centerline as the axis. The embankment has a height of 8 m, a top surface width of 3.6 m, and follows a horizontal-to-vertical slope ratio of 1:1.5. Underneath the embankment, the ground has dimensions of 12 m in depth and 35 m in width, which can be divided into two distinct layers: an upper layer consisting of silty clay with a thickness of 8 m and a lower layer composed of silt that measures 4 m thick. The model dimensions are shown in Fig. 6a. To ensure resilience against failure stresses, the problem domain was expanded horizontally and vertically. Displacement boundary conditions were imposed at the edges of the boundary. In accordance with the Chinese code for design of railway earth structure (National Railway Administration of PRC, 2016), the track and traffic loads on the subgrade surface were simplified as a uniform load, specifically 60 kPa with an effective width of 1.7 m. The relevant calculation parameters for the subgrades are listed in Tables 6 and Table 7.

When utilizing FLAC3D6.0 for computational purposes, it is also essential to consider two material parameters, namely the bulk modulus (K) and shear modulus (G). These parameters can be derived from the compression modulus (E_s) and Poisson's ratio (v), which can be calculated using the following formulas (Davarpanah et al. 2020).

$$K = \frac{E_s}{3(1-2v)} \tag{10}$$

$$G = \frac{E_s}{2(1+v)} \tag{11}$$

The investigation of railway subgrades in this study is approached as a plane-strain problem. A representative numerical cell mesh in FLAC 3D is shown in Fig. 6b. The movement at the bottom boundary edge was constrained in both the x- and y-directions, while movement along the x-direction was fixed at the side boundaries. The problem domain was discretized into 868 nonuniform zones using four-node quadrilateral elements. A relatively fine mesh was employed within the embankment region, whereas a larger mesh was selected outside the influence zone. In this study, the soils were modeled as an elastic-plastic medium adhering to the widely utilized Mohr-Coulomb yield criterion, which has found extensive application in numerical simulations, particularly those involving random field analysis (Huang et al. 2015; Li et al. 2016; Zhang et al. 2021b). The unassociated flow rule was adopted to implement the Mohr-Coulomb failure criterion within the FLAC 3D software.

The numerical model underwent multiple cycles under geostatic stress until achieving static equilibrium. The nodal displacements obtained after achieving static equilibrium were subsequently reset to zero to ensure that the embankment settlement was solely attributable to the upper load.

To assess and analyze the impact of soil parameter variability on embankment settlement, three computational models were employed:

(1) DCM, which assumes uniform soil properties with constant values in each finite difference zone throughout the entire embankment.

(2) RVM, which accounts for vertical variability of soil parameters within the layered embankment and ignores spatial autocorrelation of soil parameters.

(3) RFM, which utilizes CMD to discretize random fields such as *K*, *G*, cohesion, friction angle, and natural density, subsequently mapping them onto the embankment model.

The determination of the number of runs is crucial in Monte Carlo simulations (MCS) to obtain converged results for probability characteristics (Huang et al. 2015; Zhang et al. 2021b). Fig. 7 demonstrates the variation in average settlement of the embankment center top surface with respect to the number of runs when N=10. It can be observed that there was a mere difference of 0.1 mm between the settlement values obtained at 200 MCS runs and those at 150 MCS runs. Hence, a reasonably converged solution can be achieved with just 150 MCS runs. Consequently, 200 MCS runs were employed for the subsequent finite difference analyses in this paper.

Results

The settlement distribution curves of the top surface of the embankment for different N values are shown in Fig. 8. In Fig. 8a (RFM-1), the horizontal SOF was minimal, and the soil parameters exhibited rapid changes along the horizontal direction, as indicated by the simulation results of the random-field analysis. Consequently, each soil parameter underwent pronounced numerical variations, resulting in a discretized settlement curve for the embankment surface. As the horizontal SOF gradually increased, there was an enhanced correlation among the soils and more gradual changes in the soil parameters along the horizontal direction, leading to a stable settlement curve for the embankment surface. The settlement curves demonstrated relatively consistent behavior. Notably, The RFM results exhibited random fluctuations within the RVM results, indicating that the influence of the horizontal SOF on the settlement deformation behavior of the embankment surface primarily manifested as variations in settlement values, with minimal impact on the morphological changes observed in the settlement curve of the embankment surface.

The probability distribution of the maximum settlement on the embankment surface for different *N* values is shown in Fig. 9. At *N* values of 10, 30, 50, 70, and 100, the corresponding maximum settlements on the top surface of the embankment were 73 mm, 56 mm, 53 mm, 46 mm, and 55 mm, respectively. A comparative analysis with the RVM revealed that RFM-1 (Fig 9a) exhibited a significantly higher probability (94%) of attaining a larger maximum settlement than that predicted by the RVM. Conversely, RFM-2 to RFM-5 (Fig 9b, c, d, e) yielded smaller settlements, with probabilities (66%, 92.5%, 96%, and 85.5%, respectively) lower than those obtained from the RVM. There is a 98.5% probability that the maximum settlement value for RFM-4 exceeds that of the DCM. Moreover, the maximum settlement values for RFM-1, RFM-2, RFM-3, and RFM-5 surpassed those of the DCM. The disparities in the maximum settlement values between the RFMs and the DCM and RVM were substantial. This underscores the criticality of accounting for spatial variability in soil parameters when estimating embankment settlements.

The settlement distribution curves for the top surface of the embankment under different *N* values are illustrated in Fig. 10, while the settlement of the embankment center is shown in

Fig. 11. Both the RFM and RVM exhibited higher settlement values than the DCM results. Specifically, the average maximum settlement for RFM-1 was 77 mm, whereas the VFM yielded an average maximum settlement of 66 mm. This discrepancy can be attributed to the limited horizontal SOF and weak autocorrelation in soil properties, leading to abrupt variations in the random field characteristics and substantial errors in discrete soil parameter estimations, resulting in larger calculated settlement values. However, the RFM is capable of incorporating the local average impact of soil parameters.

With an increase in N, the average maximum settlement values of RFM-1, RFM-2, and RFM-3 were 62 mm, 54 mm, and 51 mm, respectively. Compared with the RVM results, they decreased by 6.1%, 18.4%, and 22.9%, respectively. The difference between the settlement values of RFM-3 and RFM-4 is only 3 mm. This is likely because when N = 50 and 70, the actual horizontal SOF falls within a range of approximately 40 – 60 m, resulting in a stable random field with consistent calculation results for settlement values. However, as N increases ($N \geqslant 70$), each soil layer gradually becomes more uniform in terms of horizontal SOF distribution, leading to convergence towards an RVM approach with an approximate settlement value calculation result close to that of RVM at approximately 58 mm.

The horizontal SOF exhibited a significantly larger magnitude than the vertical SOF, which was primarily attributed to the influence of soil characteristics and environmental factors. During embankment filling, a substantial area was simultaneously formed in the horizontal direction, resulting in a more homogeneous soil profile and reduced variability. Conversely, owing to layered filling techniques, greater variability exists in the vertical direction of the embankment. Based on the settlement analysis conducted in this study, the optimal range for the horizontal SOF lies between 40 and 60 m in a loess filled embankment.

Discussion

The SOF characterizes the spatial correlation structure of soil properties. N (the correlation anisotropy) is a key parameter with significant influence. Taking the compression modulus (E_s) as an example, with $\delta_v = 0.83$ m, the simulation results of different δ_h ranges are shown in Fig. 12. When the N value is small, i.e., δ_h is small, the simulated E_s exhibits strong variability in the horizontal direction, causing dramatic changes in E_s. The RFM results show a 'point' distribution. As the δ_h range increases, the color depth of the same layer gradually shows a 'stripe' distribution. The simulated value become more uniform horizontally, the coefficient of variation decreases, the horizontal spatial variability of the soil weakens, and the soil parameters of the same soil layer tend to stabilize.

The spatial average of COV_a under different N values are shown in Fig. 13. When $N = 1$, the maximum COV_a is 0.73. For $N = 50$ and 70, the corresponding COV_a values are 0.44 and 0.42, respectively. The variation range is small, the curve is gentle, and the degree of soil variation is similar. When N increases to 500 and 2000, the COV_a decreases to 0.18 and 0.11 respectively. Consequently, the soil parameters in the same soil layer show minimal change along the horizontal direction, the RFM degenerates into the RVM.

Due to the wide range of values reported in the literature, it is crucial to determine the horizontal SOF based on site-specific investigation data rather than relying on the broad ranges from existing literature (Ching et al. 2018). Numerical results indicate that the actual horizontal SOF falls within the interval of $N = 50$ and 70, demonstrating that the random field effectively captures the spatial distribution patterns of the soil parameters and yields more accurate calculations. The corresponding horizontal SOF ranges from 41.5 to 58.1 m. Cami et al. (2020) compiled statistical data on horizontal SOF from existing literature and concluded that it ranges from nearly 0 to 100 m, with most values falling between 0 and 60 m. Phoon and Kulhawy (1999) reported that the clay's horizontal SOF ranges from 23.0 to 66.0 m, with a mean value of 44.5 m based on corrected CPT tip resistance. The spatial variability of loess fill is a combination of natural variability and compaction-induced variability. (Liang et al. 2022; Yao et al.2021; Zhang et al. 2021a; Zhu and Li. 2020) Inevitably, variability in compaction density occur during the construction process. However, construction quality control specifications are enforced in the field to ensure that this variability within acceptable limits (Luo and Bathurst 2018b). Field measurements conducted by Nishimura et al. (2010) revealed significantly high values of *N* for soil strength in constructed fills. Extensive flood irrigation of farmland since 2003 has led to changes in embankment fill parameters. Consequently, the horizontal SOF aligns with the range observed for natural clay deposits, exhibiting consistent orders of magnitude but with distinct specific values. It is important to note that this outcome solely stems from numerical analysis, and further validation through extensive field test data is warranted.

Consequently, $N = 70$ was selected as the optimal analytical value. The measured values of the embankment surface settlement at the centerline of the DCM, RVM, and RFM were 35 mm, 66 mm, and 51 mm, respectively. In the DCM approach, a uniform soil composition is assumed throughout the entire embankment fill by assigning fixed values to all soil parameters. This oversimplification disregards spatial variations in these parameters and leads to underestimated calculation results. Conversely, the RVM method incorporates diverse values of soil parameters within each layer while assuming consistency across that specific layer. Currently, consideration of soil parameter inhomogeneity is currently limited to the vertical direction, neglecting its variability along the horizontal direction. This constraint impedes the accurate characterization of spatial variations in soil parameters. By incorporating both vertical and horizontal variations in the soil parameters, the RFM yields more realistic calculation outcomes. In fact, the RVM can be considered a special case of the RFM, that is, the SOF of soil parameters is considered to be infinite. However, in reality, the SOF of soil parameters is usually smaller than geo-structures scales, particularly for vertical fluctuations. This result is reasonable since the RFM accounts for local averaging effects on soil parameters (Cheng et al. 2019), which significantly reduces scatter in settlement analysis.

Random fields can effectively depict the spatial variability of soil parameters, thereby accounting for uncertain spatial variations in geotechnical materials and accurately representing the stochastic characteristics of soil materials. (Cheng et al. 2019; Deng et al. 2022; Foye and Soong 2010; Li et al. 2016; Zhang et al. 2024). Consequently, employing RFM to estimate soil parameters offers a rational and viable approach for the precise calculation of embankment settlement. The results provide unequivocal evidence that the heterogeneity of loess-filled embankments primarily contributes to the variability in settlements. This approach represents an initial stride towards a more accessible simulation methodology for design.

Conclusion

(1) The semivariogram method was used to determine the vertical SOF of the embankment fill. The range of vertical SOF values derived from CPT data falls within 0.68 and 0.84 m, whereas for borehole test data, it ranges between 0.71 and 0.99 m, slightly higher than the

former range. Sampling spacing and the number of samples influenced the vertical SOF.

(2) Due to layered filling during embankment construction, strong variability is observed in the vertical direction of the embankment fill layer, whereas in the horizontal direction, it often forms a single large area. The embankment fill layer was relatively uniform and exhibited a small variability in the horizontal direction. The horizontal SOF is significantly larger than the vertical SOF. The settlement analysis revealed a horizontal SOF ranging between 40 and 60 m for the loess-filled embankment.

(3) A comparison the DCM, RVM, and RFM results indicated a settlement value of 35mm for the embankment surface at the centerline in the DCM. However, this model completely disregards the spatial variability of the soil parameters, resulting in underestimated calculation s. The RVM only accounts for the heterogeneity of soil parameters along the depth direction, neglecting their variability along the horizontal direction. hence yielding a settlement of 66 mm. In contrast, RFM incorporated both vertical and horizontal variabilities of soil parameters into its analysis and provided a more accurate characterization of their spatial distribution, leading to more reasonable calculation results.

Acknowledgements

This work was supported the National Natural Science Foundation of China (Grant Nos. 52268058;51868038); Tianyou Youth Talent Lift Program of Lanzhou Jiaotong University; Gansu Provincial Natural Science Foundation (20JR10RA235); Special Funds for Guiding Local Scientific and Technological Development by The Central Government(22ZY1QA005). Gansu Provincial Department of Education Industrial Support Program Project, China(2023CYZC-34).

References

Alamanis N, Dakoulas P (2021) Simulation of random fields of soil properties by the local average subdivision method and engineering applications. Energy Syst 12:841-861. https://doi.org/10.1007/s12667-019-00362-y

Bian XC, Duan X, Li W, Jiang JQ (2021) Track settlement restoration of ballastless high-speed railway using polyurethane grouting: Full-scale model testing. Transp Geotech 26: 100381. https://doi.org/10.1016/j.trgeo.2020.100381

Cami B, Javankhoshdel S, Phoon KK, Ching JY (2020) Scale of fluctuation for spatially varying soils: estimation methods and values. ASCE-ASME J Risk Uncertain Eng Syst Part A Civ Eng 6(4):03120002. https://doi.org/10.1061/AJRUA6.0001083

Chai JC, N Miura (2002) Traffic-load-induced permanent deformation of road on soft subsoil. J Geotech Geoenviron Eng 128(11):907-916. https://doi.org/10.1061/(ASCE)1090-0241(2002)128:11(907).

Charoenwong C, Connolly DP, Woodward PK, Galvín P, Costa PA (2022) Analytical forecasting of long-term railway track settlement. Comput Geotech 143:104601. https://doi.org/10.1016/j.compgeo.2021.104601

Chen RP, Chen JM, Zhao X, Bian XC, Chen YM (2014) Cumulative settlement of track subgrade in high-speed railway under varying water levels. Int J Rail Transp 2(4):205-220. https://doi.org/10.1080/23248378.2014.959083

Chen RP, Jiang P, Ye XW, Bian XC. (2016) Probabilistic analytical model for settlement risk assessment of high-speed railway subgrade. J Perform Constr Fac 30(3):04015047. https://doi.org/10.1061/(ASCE)CF.1943-5509.0000789

Cheng HZ, Chen J, Chen RP, Chen GL. (2019). Comparison of modeling soil parameters using random variables and random fields in reliability analysis of tunnel face. Int J Geomech 19(1):04018184. https://doi.org/10.1061/(ASCE)GM.1943-5622.0001330

Ching, J., Wu, T. J., Stuedlein, A. W., Bong, T. (2018). Estimating horizontal scale of fluctuation with limited CPT soundings. Geosci Front 9(6):1597-1608. https://doi.org/10.1016/j.gsf.2017.11.008

Cho SE (2007) Effects of spatial variability of soil properties on slope stability. Eng Geol 92(3-4):97-109. https://doi.org/10.1016/j.enggeo.2007.03.006

Clark I (1979) Practical Geostatistics. Applied Science, London.

Dasaka SM, Zhang LM (2012) Spatial variability of in situ weathered soil. Géotechnique, 62(5):375-384. https://doi.org/10.1680/geot.8.P.151.3786

Davarpanah SM, Bar N, Török Á, Tarifard A, Vásárhelyi B (2020) Determination of Young's modulus and Poisson’s ratio for intact stratified rocks and their relationship with uniaxial compressive strength. Aust Geomech J 55(4):101-118.

Deng ZP, Pan M, Niu JT, Jiang SH (2022). Full probability design of soil slopes considering both stratigraphic uncertainty and spatial variability of soil properties. Bull Eng Geol Environ 81(5):195. https://doi.org/10.1007/s10064-022-02702-2

Elkateb T, Chalaturnyk R, Robertson PK (2003) An overview of soil heterogeneity: quantification and implications on geotechnical field problems. Can Geotech J 40(1):1-15. https://doi.org/10.1139/t02-090

Feng SX, Lei HY. (2022) A settlement prediction model considering tidal loading and traffic loading of soft soil subgrade. Comput Geotech 144:104639.

https://doi.org/10.1016/j.compgeo.2022.104639

Fenton GA (1999) Estimation for stochastic soil models. J Geotech Geoenviron Eng 125(6): 470-485. https://doi.org/10.1061/(ASCE)1090-0241(1999)125:6(470)

Fenton G A, Griffiths DV (2003) Bearing-capacity prediction of spatially random c−φ soils. Can Geotech J 40 (1): 54-65. https://doi.org/10.1139/t02-086

Foye KC, Soong TY. (2010) Simulating differential settlement of landfill foundations using random fields. InGeoFlorida: Advances in Analysis, Modeling & Design, 2042-2051. https://doi.org/10.1061/41095(365)207

Fenton G A, Griffiths DV (2007) Random field generation and the local average subdivision method. Probabilistic methods in geotechnical engineering. Vienna: Springer Vienna.

Gomes FP, Garcia CH (2002) Estatrstica aplicada a experimentos agronomicos e florestais: exposição com exemplos e orientações para uso de aplicativos. Piracicaba, SP: FEALQ, 309.

Gong WP, Tang HM, Juang CH, Wang L (2020) Optimization design of stabilizing piles in slopes considering spatial variability. Acta Geotech 15:3243-3259. https://doi.org/10.1007/s11440-020-00960-6

Harr ME (1987) Reliability-based design in civil engineering, McGraw-Hill.

Huang HW, Gong WP, Khoshnevisan S, Juang CH, Zhang DM, Wang L (2015). Simplified procedure for finite element analysis of the longitudinal performance of shield tunnels considering spatial soil variability in longitudinal direction. Comput Geotech 64:132-145. https://doi.org/10.1016/j.compgeo.2014.11.010

Huang SP, Quek ST, Phoon KK (2001) Convergence study of the truncated Karhunen–Loeve expansion for simulation of stochastic processes. Int J Numer Methods Eng 52(9):1029-1043.

https://doi.org/10.1002/nme.255

Jiang SH, Huang JS (2016) Efficient slope reliability analysis at low-probability levels in spatially variable soils. Comput Geotech 75: 18-27. https://doi.org/10.1016/j.compgeo.2016.01.016.

Juang CH, Dijkstra T, Wasowski J, Meng XM (2019) Loess geohazards research in China: advances and challenges for mega engineering projects. Eng Geol 251:1-10. https://doi.org/10.1016/j.enggeo.2019.01.019

Kalantari AR, Johari A, Zandpour M, Kalantari M (2023). Effect of spatial variability of soil properties and geostatistical conditional simulation on reliability characteristics and critical slip surfaces of soil slopes. Transp Geotech 39:100933. https://doi.org/10.1016/j.trgeo.2023.100933

Kerry R, Oliver MA (2011) Soil geomorphology: Identifying relations between the scale of spatial variation and soil processes using the variogram. Geomorphology130(1-2):40-54. https://doi.org/10.1016/j.geomorph.2010.10.002

Kim JM, Sitar N (2013) Reliability approach to slope stability analysis with spatially correlated soil properties. Soils Found 53 (1):1-10. https://doi.org/10.1016/j.sandf.2012.12.001

Li JH, Zhou Y, Zhang LL, Tian Y, Cassidy MJ, Zhang LM (2016) Random finite element method for spudcan foundations in spatially variable soils. Eng Geol 205:146-155. https://doi.org/10.1016/j.enggeo.2015.12.019

Li TZ, Gong WP, Tang HM (2021) Three-dimensional stochastic geological modeling for probabilistic stability analysis of a circular tunnel face. Tunn Undergr Sp Tech 118:104190. https://doi.org/10.1016/j.tust.2021.104190

Liang YH, Shui WH, Lu SF (2022) Field practice and ground settlement behaviors of a land creation case in loess area of China. Bull Eng Geol Environ 81(11):462. https://doi.org/10.1007/s10064-022-02964-w

Lloret-Cabot M, Fenton GA, Hicks MA (2014) On the estimation of scale of fluctuation in geostatistics. Georisk Assess Manag Risk Eng Syst Geohazards 8(2):129-140. https://doi.org/10.1080/17499518.2013.871189

Lu Z, Fang R, Chen LH, She JB, Xian SH (2020) Long-term deformation of highway subgrade under coupling effect of traffic load and drying-wetting cycles. Int J Geomech 20(2): 04019168. https://doi.org/10.1061/(ASCE)GM.1943-5622.0001568

Luo H, Wu FQ, Chang JY, Xu JB (2018a) Microstructural constraints on geotechnical properties of Malan loess: a case study from Zhaojiaan landslide in Shaanxi province, China. Eng Geol 236:60-69. https://doi.org/10.1016/j.enggeo.2017.11.002

Luo N, Bathurst RJ (2018b) Deterministic and random FEM analysis of full-scale unreinforced and reinforced embankments. Geosynth Int 25(2):164-179. https://doi.org/10.1680/jgein.17.00040

Mantoglou A, Wilson JL (1982) The turning bands method for simulation of random fields using line generation by a spectral method. Water Resour Res 18(5):1379-1394. https://doi.org/10.1029/WR018i005p01379

National Railway Administration of the People's Republic of China. (2016) Code for design of railway earth structure. Beijing: China Railway Press; Chinese.

Nguyen TS, Likitlersuang S, Jotisankasa A (2019) Influence of the spatial variability of the root cohesion on a slope-scale stability model: a case study of residual soil slope in Thailand. Bull

Eng Geol Environ 78:3337-3351. https://doi.org/10.1007/s10064-018-1380-9

Nguyen TS, Likitlersuang S (2021) Influence of the spatial variability of soil shear strength on deep excavation: A case study of a Bangkok underground MRT station. Int J Geomech 21(2): 04020248. https://doi.org/10.1061/(ASCE)GM.1943-5622.0001914

Nishimura, S. ichi, Murakami, A., Matsuura, K. (2010). Reliability-based design of earth-fill dams based on the spatial distribution of strength parameters. Georisk Assess Manag Risk Eng Syst Geohazards 4(3):140-147. https://doi.org/10.1080/17499511003676655

Onyejekwe S, Kang X, Ge L (2016) Evaluation of the scale of fluctuation of geotechnical parameters by autocorrelation function and semivariogram function. Eng Geol 214(Nov):43-49. https://doi.org/10.1016/j.enggeo.2016.09.014

Pan YT, Liu Y, Tyagi A, Lee, FH, Li DQ (2021) Model-independent strength-reduction factor for effect of spatial variability on tunnel with improved soil surrounds. Géotechnique 71(5):406-422. https://doi.org/10.1680/jgeot.19.P.056

Pardo-Igúzquiza E, Chica-Olmo M (1993) The Fourier Integral Method: An efficient spectral method for simulation of random fields. Math Geol 25:177-217 https://doi.org/10.1007/BF00893272

Pebesma EJ (2004) Multivariable geostatistics in S: the gstat package. Comput Geotech 30(7):683-691. https://doi.org/10.1016/j.cageo.2004.03.012

Peduto D, Huber M, Speranza G, Ruijven J, Cascini L (2017) DInSAR data assimilation for settlement prediction: case study of a railway embankment in the Netherlands. Can Geotech J 54(4):502-517. https://doi.org/10.1139/cgj-2016-0425

Peng X, Li DQ, Cao ZJ, Gong WP, Juang CH (2017) Reliability based robust geotechnical design using Monte Carlo simulation. Bull Eng Geol Environ 76(3):1217-1227. https://doi.org/10.1007/s10064-016-0905-3

Phoon KK, Kulhawy FH (1999) Characterization of geotechnical variability. Can Geotech J 36 (4):612-624. https://doi.org/10.1139/t99-038

Phoon K K, Quek ST, An P (2003) Identification of statistically homogeneous soil layers using modified Bartlett statistics. J Geotech Geoenviron 129 (7):649-659. https://doi.org/10.1061/(ASCE)1090-0241(2003)129:7(649)

Phoon KK, Ching J (2015) Risk and reliability in geotechnical engineering. CRC Press, New York.

Press WH (2007) Numerical recipes 3rd edition: The art of scientific computing. Cambridge university press.

Sasanian S, Soroush A, Jamshidi Chenari R. (2019) Effect of sampling interval on the scale of fluctuation of CPT profiles representing random fields. Int J Civ Eng 17:871-880. https://doi.org/10.1007/s40999-018-0371-3

Simões JT, Neves LC, Antão AN, Guerra NM (2020) Reliability assessment of shallow foundations on undrained soils considering soil spatial variability. Comput Geotech 119(Mar):103369. https://doi.org/10.1016/j.compgeo.2019.103369

Singh A, Lee KL (1970) Variability in soil parameters, Proceedings 8th Annual Engineering Geology and Soils Engineering Symposium, Idaho, 159-185.

Sun ZH, Tan WX, Wu TY (2022) Effect of spatial variability of cement-treated soil on the roughness of airport pavement. Int J Pavement Res Technol 15:1118-1126. https://doi.org/10.1007/s42947-021-00076-4

Tian H, Li DQ, Cao ZJ, Du W (2023) Auxiliary Bayesian updating of embankment settlement based on finite element model and response surface method. Eng Geol 323:107244. https://doi.org/10.1016/j.enggeo.2023.107244

Vaillancourt M, Houy L, Perraton D, Breysse D (2015) Variability of subgrade soil rigidity and its effects on the roughness of flexible pavements: A probabilistic approach. Mater Struct 48:3527-3536. https://doi.org/10.1617/s11527-014-0419-z

Vanmarcke EH (1977) Probabilistic modeling of soil profiles. J Geotech Eng Div 103 (11): 1227-1246. https://doi.org/10.1061/AJGEB6.0000517

Vanmarcke EH (1983) Random fields: analysis and synthesis. MIT Press, Cambridge.

Wang CH, Wang K, Tang, DF, Hu BL, Kelata Y (2022) Spatial random fields-based Bayesian method for calibrating geotechnical parameters with ground surface settlements induced by shield tunneling. Acta Geotech 17:1503-1519. https://doi.org/10.1007/s11440-021-01407-2

Wang Y, Zhao TY, Phoon KK (2018) Direct simulation of random field samples from sparsely measured geotechnical data with consideration of uncertainty in interpretation. Can Geotech J 55(6):862-880. https://doi.org/10.1139/cgj-2017-0254

Wilding LP, Drees LR (1983) Spatial variability and pedology. Developments in Soil Science, 11(Part A): 83-116. https://doi.org/10.1016/S0166-2481(08)70599-3

Xiao JH, Shan J, Wu N, Liu MB, Wan HY, Sun SQ, Long XY. (2023) Long-term settlement of metro viaduct piers: A case study in Shanghai soft soil. Transp Geotech 42:101075. https://doi.org/10.1016/j.trgeo.2023.101075

Yang Y, Wang P, Brandenberg S J. (2022). An algorithm for generating spatially correlated random fields using Cholesky decomposition and ordinary kriging. Comput Geotech

147:104783. https://doi.org/10.1016/j.compgeo.2022.104783

Yang ZY, Nie JY, Peng X, Tang D, Li XY (2021) Effect of random field element size on reliability and risk assessment of soil slopes. Bull Eng Geol Environ 80:7423-7439. https://doi.org/10.1007/s10064-021-02422-z

Yao YG, Zhang YC, Zhao Y, Bai YF, Zhang SN, Cao CM. (2021) The evaluation of artificial filling in loess areas by in-situ tests based on statistical analysis. Environ Earth Sci 80:438. https://doi.org/10.1007/s12665-021-09729-w

Zhai WM. (2007) Vehicle-track coupling dynamics. Beijing: Science Press; Chinese.

Zhang LX, Qi SW, Yu YT, Zhang YG, Li ZQ, Hou XK, Ma LN, Zou Y, Guo SF, Peng JB (2021a) A comparative study on the physical properties of natural sedimentary loess and manual filling compacted loess. Environ Earth Sci 80:721. https://doi.org/10.1007/s12665-021-10047-4

Zhang LL, Zhang LM, Tang WH (2008). Similarity of soil variability in centrifuge models. Can Geotech J 45 (8):1118-1129. https://doi.org/10.1139/T08-066

Zhang JZ, Huang HW, Zhang DM, Zhou ML, Tang C, Liu DJ (2021b) Effect of ground surface surcharge on deformational performance of tunnel in spatially variable soil. Comput Geotech 136:104229. https://doi.org/10.1016/j.compgeo.2021.104229

Zhang JZ, Zhang DM, Huang HW, Phoon KK, Tang C, Li G (2022) Hybrid machine learning model with random field and limited CPT data to quantify horizontal scale of fluctuation of soil spatial variability. Acta Geotech 17:1129-1145. https://doi.org/10.1007/s11440-021-01360-0

Zhang SC, Wang YQ, Gao QD, Ma XB, Zhou HX, Wang ZF (2024) Probabilistic analysis of ground settlement induced by tunnel excavation in multilayered soil considering spatial variability. Comput Geotech 165:105951. https://doi.org/10.1016/j.compgeo.2023.105951

Zhao HF, Zhang LM, Xu Y, Chang DS (2013) Variability of geotechnical properties of a fresh landslide soil deposit. Eng Geol 166:1-10.https://doi.org/10.1016/j.enggeo.2013.08.006

Zhao M, Chen LY, Wang SY, Wu HG (2020) Experimental study of the microstructure of loess on its macroscopic geotechnical properties of the Baozhong railway subgrade in Ningxia, China. Bull Eng Geol Environ 79:4829-4840. https://doi.org/10.1007/s10064-020-01816-9

Zhou SH, Wang BY, Shan Y (2020) Review of research on high-speed railway subgrade settlement in soft soil area. Railway Eng Sci 28:129-145.https://doi.org/10.1007/s40534-020-00214-x

Zhu H, Zhang LM, Zhang LL, Zhou CB (2013) Two-dimensional probabilistic infiltration analysis with a spatially varying permeability function. Comput Geotech 48:249-259. https://doi.org/10.1016/j.compgeo.2012.07.010

Zhu CH, Li N (2020) Ranking of influence factors and control technologies for the post-construction settlement of loess high-filling embankments. Comput Geotech 118(Feb.):103320. https://doi.org/10.1016/j.compgeo.2019.103320

Zhuang Y, Wang KY (2016). Finite-element analysis on the effect of subsoil in reinforced piled embankments and comparison with theoretical method predictions. Int J Geomech 16(5): 04016011. https://doi.org/10.1061/(ASCE)GM.1943-5622.0000628

Tables

Table 1 Relationship between range of influence and scale of fluctuation. (Onyejekwe et al. 2016)

Model	Mathematical Function	SOF
Spherical	$\gamma(h) = C_0 + C\left(\frac{3h}{2a} - \frac{h^3}{2a^3}\right) h \leq a$ $\gamma(h) = C_0 + C\ h \geq a$	$3a/4$
Gaussian	$\gamma(h) = C_0 + C\left(1 - e^{-\frac{h^2}{a^2}}\right)$	$\pi^{0.5}a$
Exponential	$\gamma(h) = C_0 + C\left(1 - e^{-\frac{h}{a}}\right)$	$2a$

a = range of influence; h = lag length

Table 2 Values of Physical indices of soils

Soil layer	Water content (%)	Natural density ($g \cdot cm^{-3}$)	Specific gravity	Void ratio	Liquid limit (%)	Plastic limit (%)
Silty clay	23.15	1.81	2.64	1.07	31.35	20.83
Silt	24.79	1.90	2.60	1.01	26.71	17.94

Table 3 Physical and mechanical parameters of embankment fill layer

Depth(m)	Water content (%)	Natural density (g·cm^{-3})	Void ratio	Compression modulus (MPa)	Cohesion (kPa)	Friction angle (°)
0.5	13.25	1.83	0.88	11.51	23	24
1.0	12.27	1.66	1.01	16.32	45	29
1.5	10.32	1.73	0.81	5.23	42	18
2.0	13.73	1.63	0.86	3.52	50	24
2.5	12.15	1.71	0.74	4.61	40	25
3.0	12.24	1.76	0.76	4.21	30	18
3.5	15.56	1.88	1.11	5.23	25	19
4.0	14.37	1.83	1.07	3.51	50	25
4.5	13.89	1.88	0.83	3.26	40	29
5.0	15.21	1.79	0.94	2.51	35	20
5.5	12.12	1.73	0.94	7.01	50	21
6.0	12.91	1.81	1.05	6.41	25	19
6.5	10.22	1.87	1.08	8.24	50	18
7.0	11.93	1.92	0.95	16.13	16	26
7.5	11.12	1.94	1.04	11.51	21	28
8.0	9.68	1.76	0.98	18.52	25	21

Table 4 Vertical SOFs of physical and mechanical parameters

parameter	K330 + 000 (m)	K330 + 100 (m)	K330 + 150 (m)	K330 + 200 (m)
Water content	0.83	0.84	0.99	0.75
Natural density	0.85	0.84	0.91	0.73
Void ratio	0.86	0.79	0.88	0.71
Cohesion	0.88	0.81	0.86	0.78
Friction angle	0.85	0.83	0.95	0.74
Compression modulus	0.93	0.91	0.95	0.74
Variation range	0.83～0.93	0..79～0.91	0.86～0.99	0.71～0.78
Mean value	0.87	0.84	0.92	0.74
Penetration resistance (CPT)	0.78	0.74	0.84	0.68

Table 5 COV for physical and mechanical parameters

parameter	COV_p (%)	variability	COV_a(%)				variability
			K330 +000	K330 +100	K330+150	K330 +200	
Water content	13.8	medium	4.4	4.5	4.8	4.2	low
Natural density	5.0	low	1.6	1.6	1.7	1.5	low
Void ratio	12.4	medium	4.1	3.9	4.1	3.7	low
Cohesion	65.3	very high	21.7	20.8	21.4	20.4	high
Friction angle	33.6	very high	10.9	10.8	11.6	10.2	medium
Compression modulus	17.5	medium	6.0	5.9	6.0	5.3	low

Table 6 Pertinent calculation parameters for embankment fill

Depth(m)	Bulk modulus (MPa)	Shear modulus (MPa)	Cohe-sion (kPa)	Friction angle (°)	Natural density ($kg{\cdot}m^{-3}$)
0.5	7.99	4.57	23	24	1800
1.0	11.33	6.48	45	29	1660
1.5	3.63	2.08	42	18	1730
2.0	2.44	1.40	50	24	1630
2.5	3.20	1.83	40	25	1710
3.0	2.92	1.67	30	18	1760
3.5	3.63	2.08	25	19	1880
4.0	2.44	1.39	50	25	1830
4.5	2.26	1.29	40	29	1880
5.0	1.74	1.00	35	20	1790
5.5	4.87	2.78	50	21	1730
6.0	4.45	2.54	25	19	1800
6.5	5.72	3.27	50	18	1870
7.0	11.20	6.40	16	26	1920
7.5	7.99	4.57	21	28	1940
8.0	12.86	7.35	25	21	1760

Table 7 Pertinent calculation parameters for ground

Soil layer	Bulk modulus (MPa)	Shear modulus (MPa)	Cohe-sion (kPa)	Friction angle (°)	Natural density ($kg{\cdot}m^{-3}$)
Silty clay	10.42	5.95	35	25	1810
Silt	14.49	7.87	20	29	1900

Figures

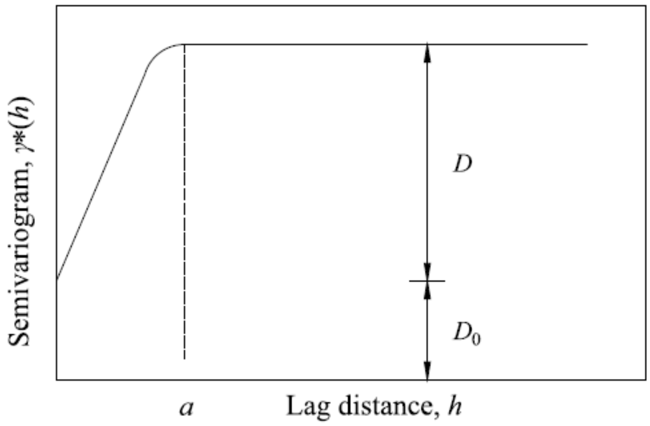

Fig. 1 Typical spherical theoretical semivariogram.

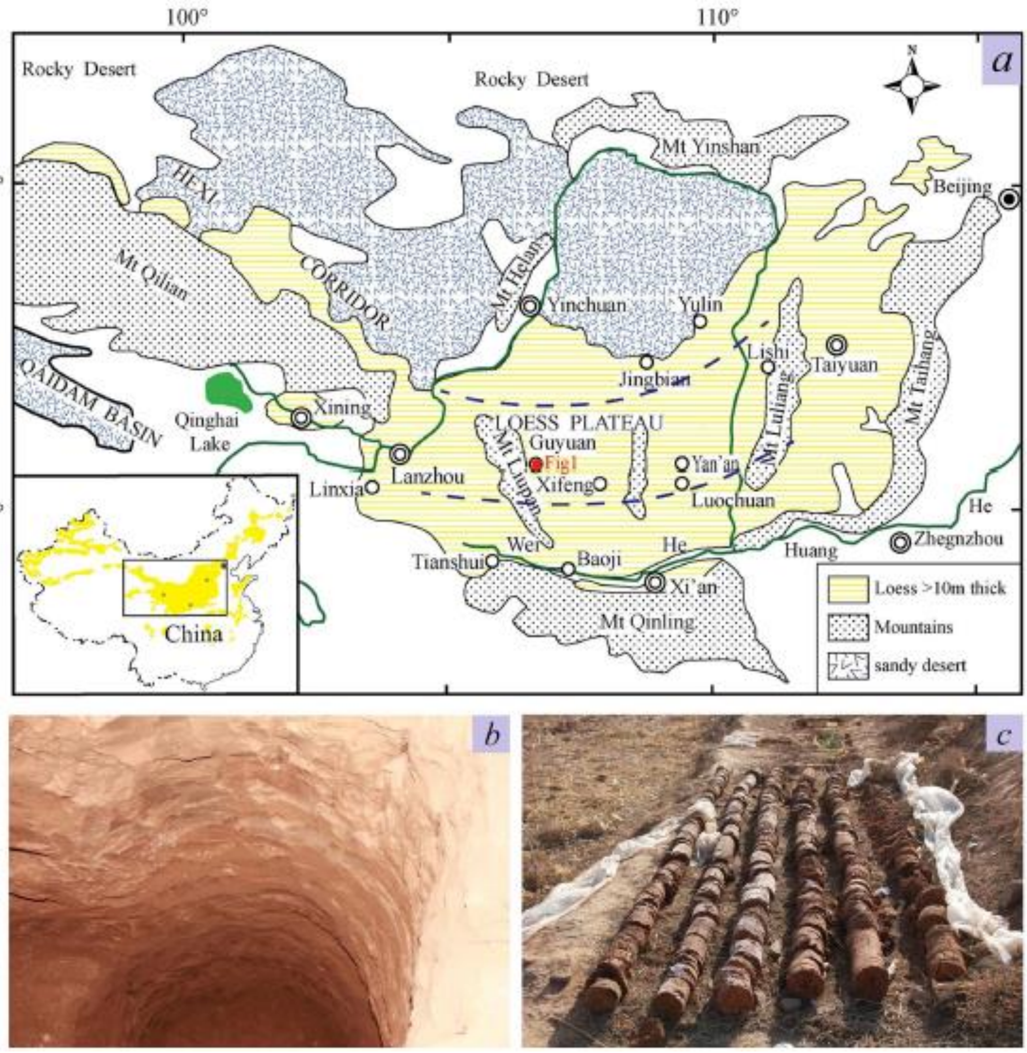

Fig. 2 a The location of the study area (after Luo et al. 2018). b Inspection pit test. c Borehole core samples.

Fig. 3 Subgrade disease of Baozhong railway. a Cracks at K330+000 section; b Cracks at K330+200 section; c Uneven track at K330+200 section; d Uneven track at K331+250 section.

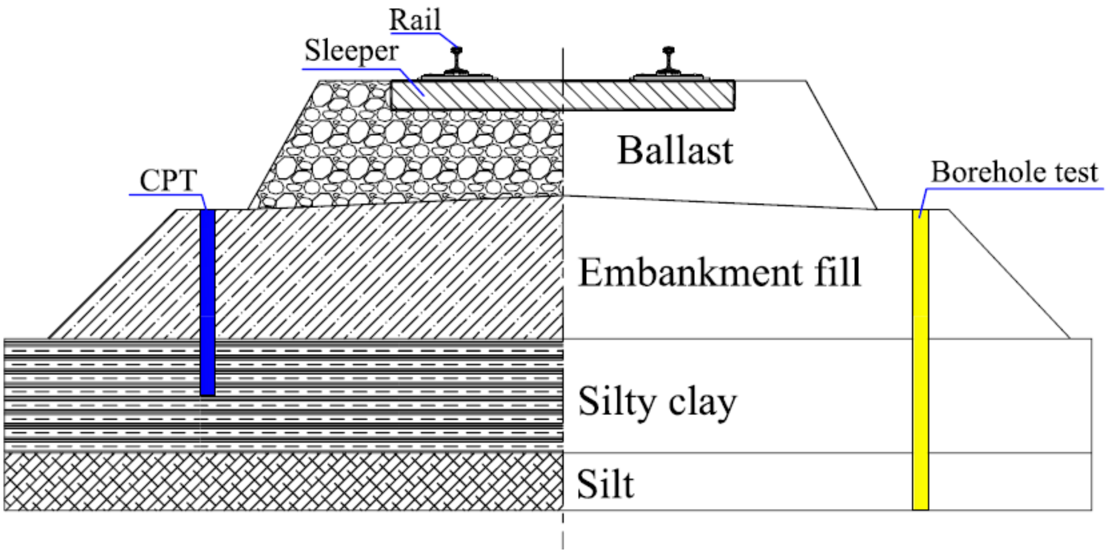

Fig. 4 CPT and borehole tests location diagram.

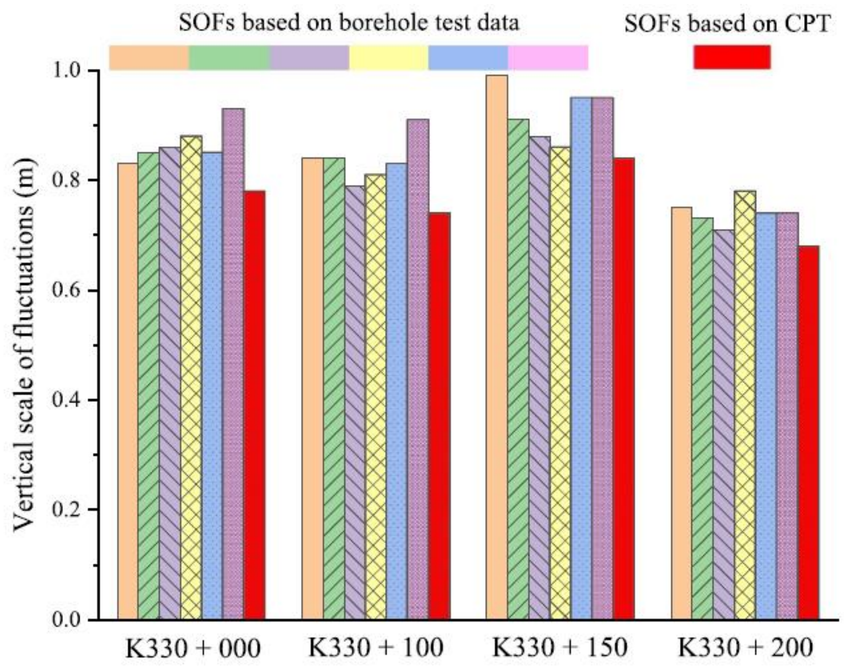

Fig. 5 Vertical SOFs of physical and mechanical parameters computed based on borehole test data and penetration resistance of CPT.

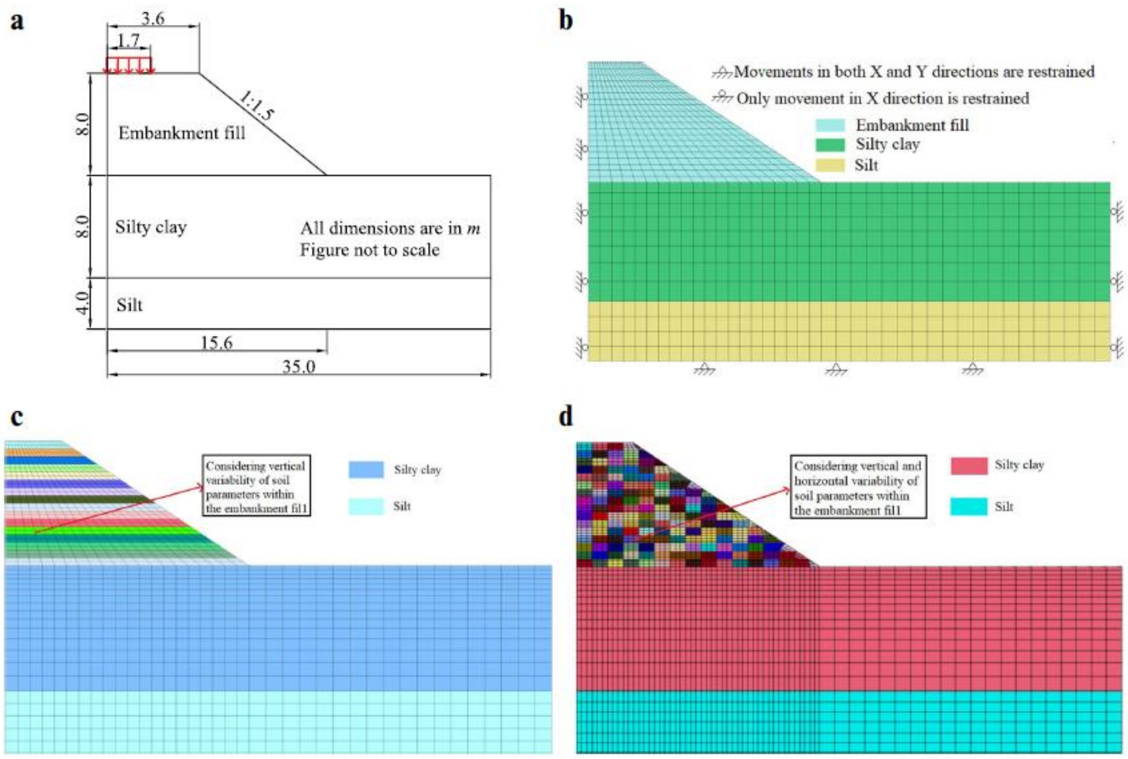

Fig. 6 Numerical model of subgrade mechanics. a Dimensions of the subgrade model; b Deterministic calculations model (DCM); c Random vertical model (RVM); d Random field model (RFM).

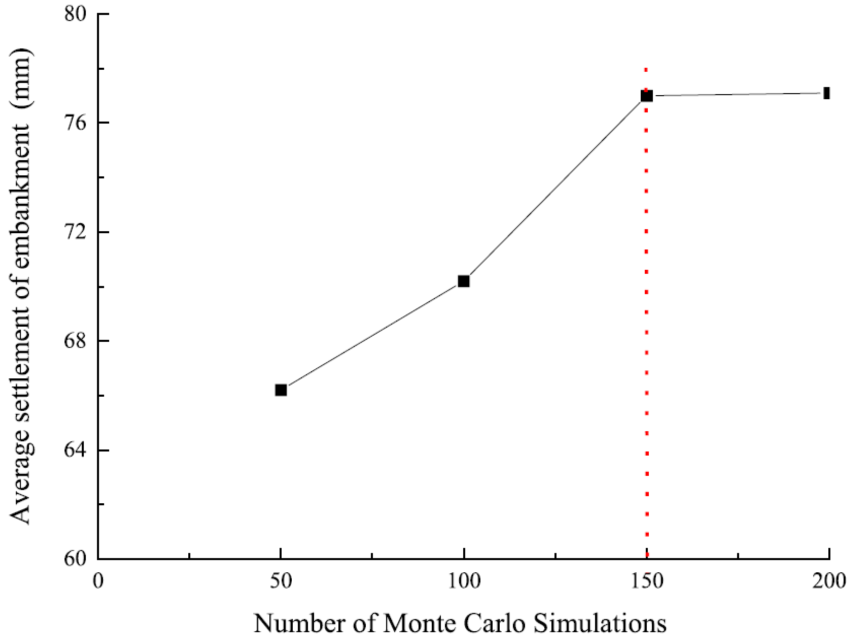

Fig. 7 The converging trend of average settlement of embankment center top surface (N=10).

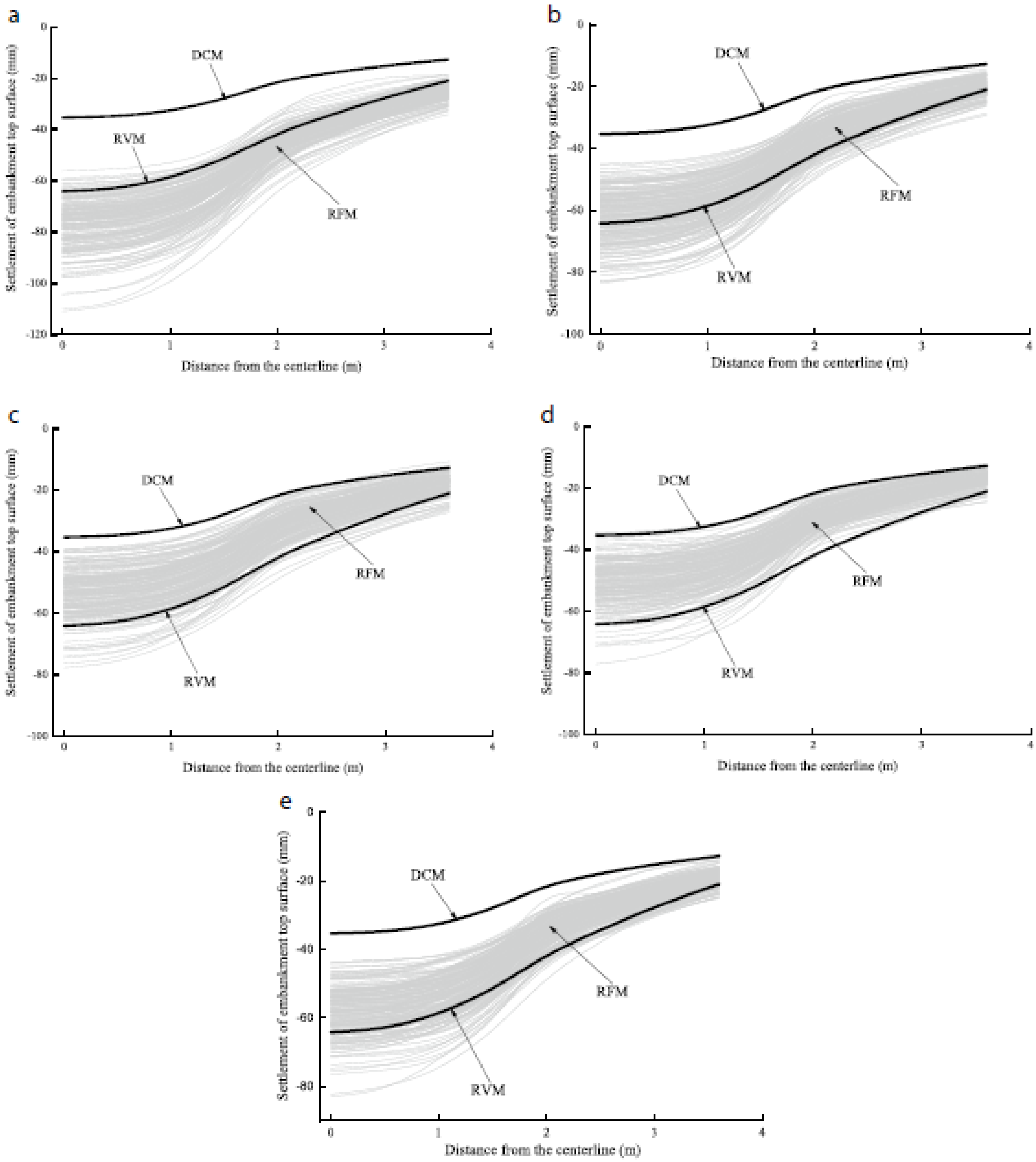

Fig. 8 The settlement distribution curves of embankment top surface under different N values.

a RFM-1 (N=10); b RFM-2 (N=30); c RFM-3 (N=50); d RFM-4 (N=70); e RFM-5 (N=100).

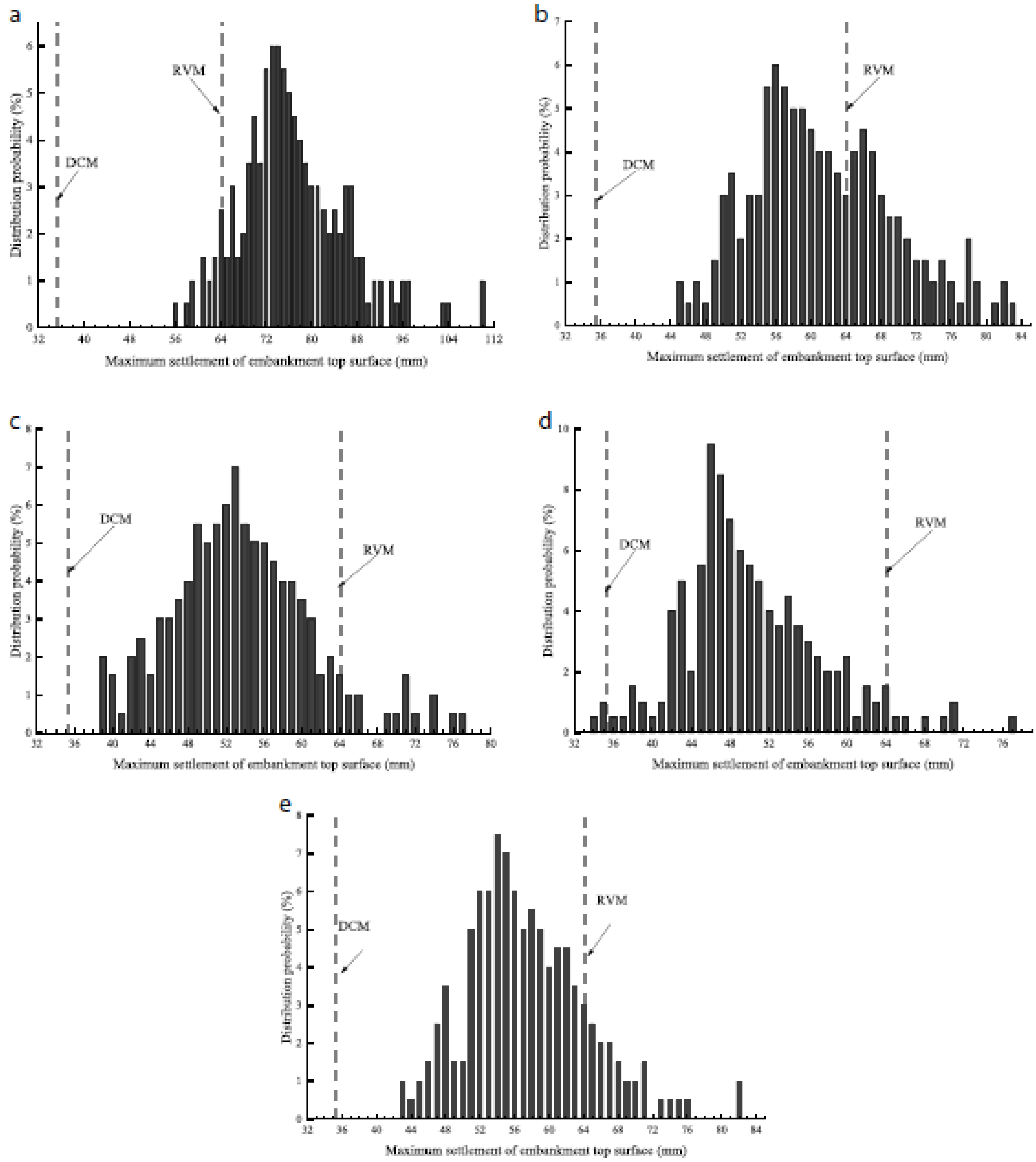

Fig. 9 Probability histograms of the maximum settlement of embankment top surface under different N values. a RFM-1 (N=10); b RFM-2 (N=30); c RFM-3 (N=50); d RFM-4 (N=70); e RFM-5 (N=100).

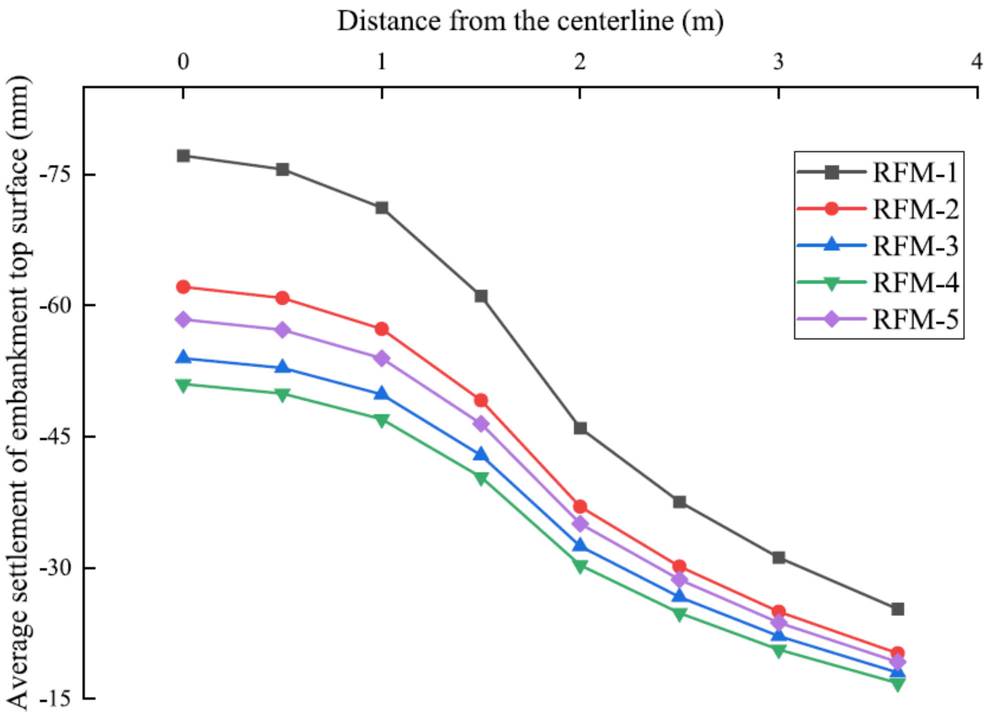

Fig. 10 The average settlement distribution curves of embankment top surface under different N values.

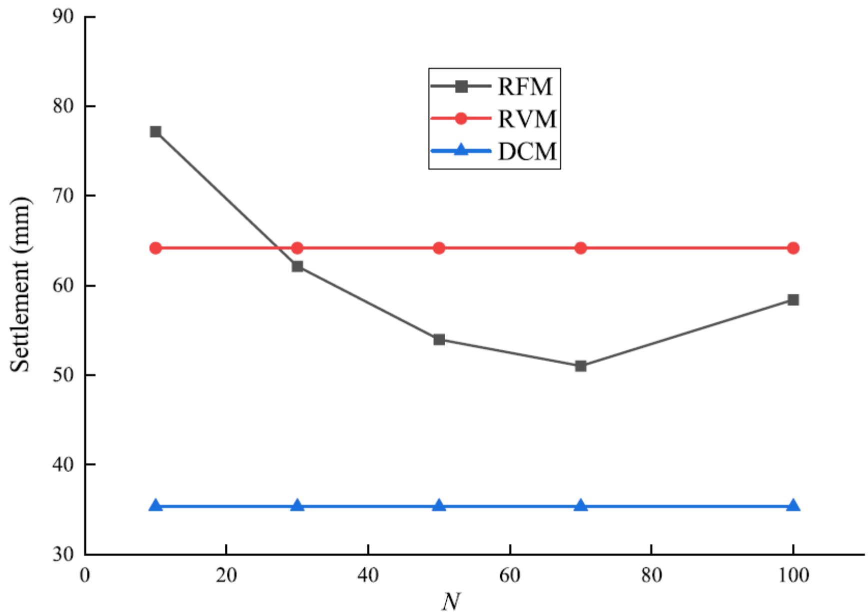

Fig. 11 The settlement distribution curves of embankment center under different N value.

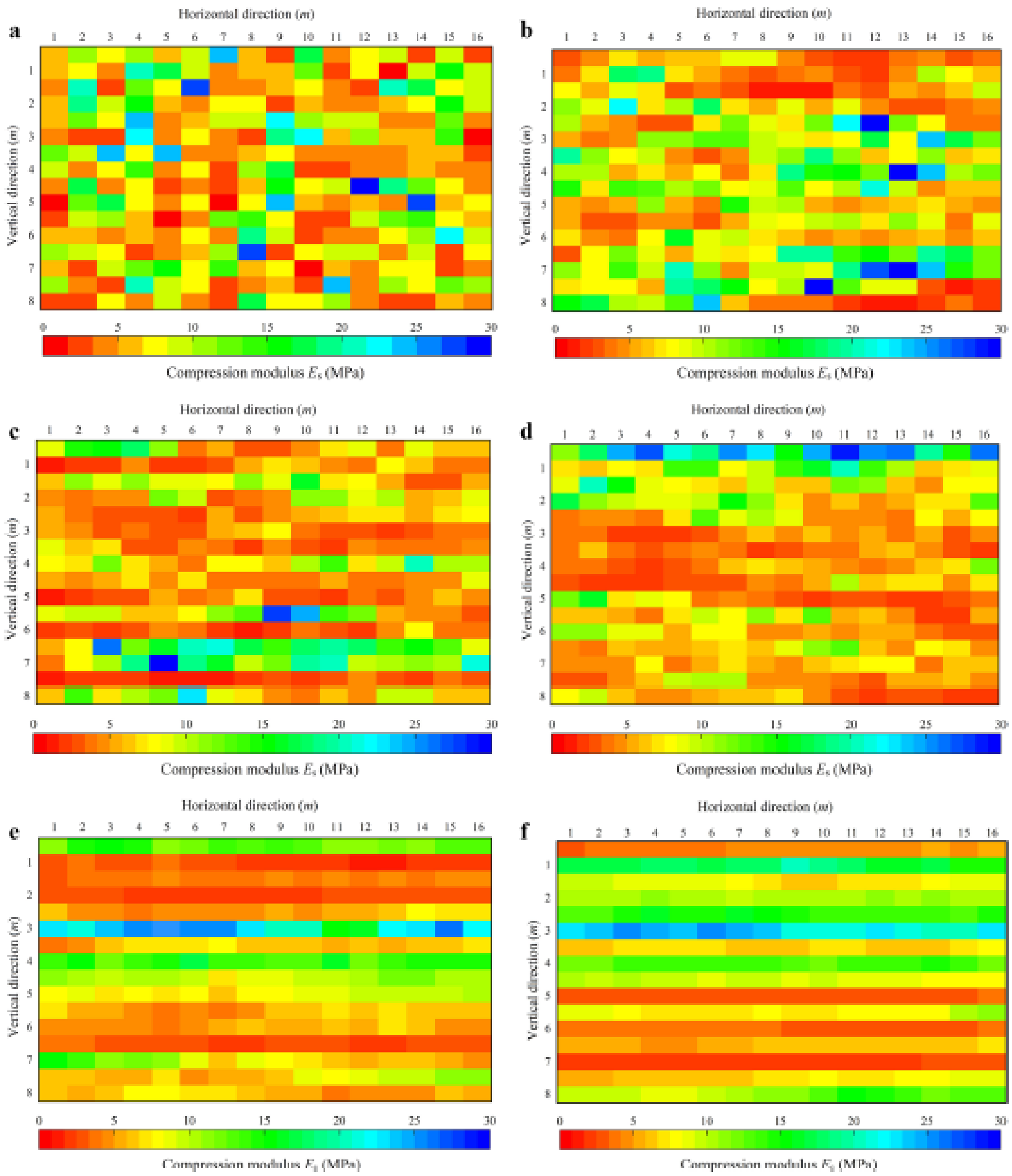

Fig. 12 The random field simulation results for compression modulus (E_S). a N=1; b N=30; c N=50; d N=70; e N=500; f N=2000.

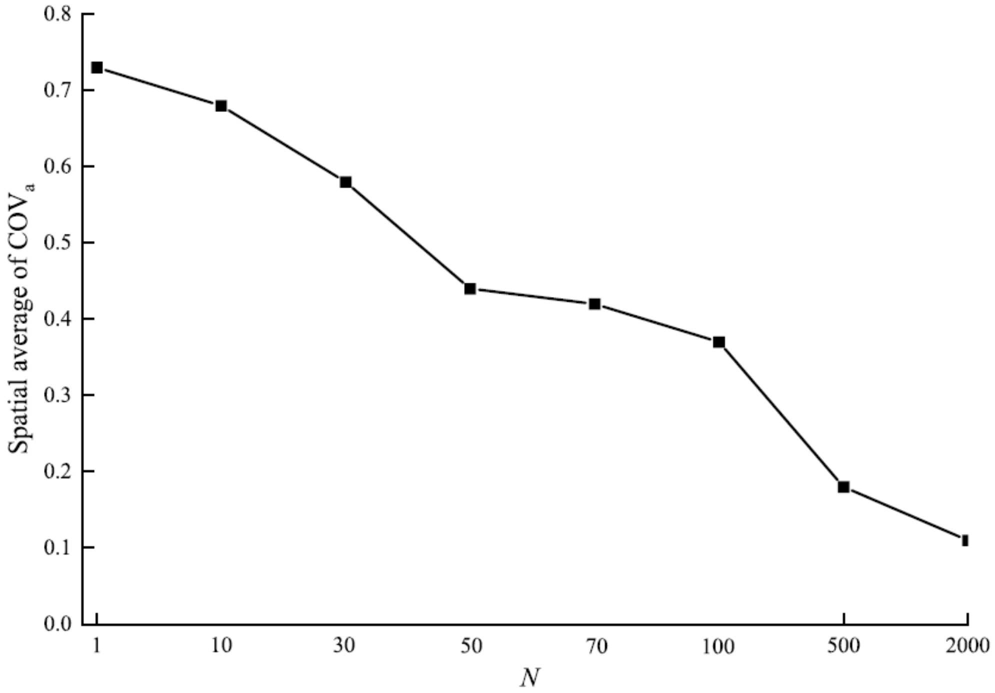

Fig. 13 The spatial average of COV_a under different N values.